

Excitation by fast atoms at very high electric field to gas-density ratios in argon

D. A. Scott* and A. V. Phelps†

Joint Institute for Laboratory Astrophysics, University of Colorado and National Institute of Standards and Technology, Boulder, Colorado 80309

(Received 6 November 1990)

Measurements of transient and steady-state light emission and of current transients from Ar at very high electric field to gas-density ratios E/n and low gas densities show that the excitation of the 811-nm lines of Ar is primarily by fast neutral Ar atoms. A drift tube with parallel-plane electrodes produces a spatially uniform electric field. Pulsed laser irradiation at 266 nm of the semitransparent cathode produces current pulses of ≈ 10 mA and ≈ 10 ns width. The time and spatial dependences of the line emission at 811 ± 1 and 750 ± 1 nm were measured for E/n in the range 280 townsend (Td) to 84 kTd at gas densities from 1.3×10^{23} to $9 \times 10^{20} \text{ m}^{-3}$, where $1 \text{ Td} = 10^{-21} \text{ V m}^2$. At $E/n < 4$ kTd the time dependence of the 811-nm emission is consistent with direct and cascade excitation due to electron collisions with Ar. At $E/n > 18$ kTd the emission transient consists of an early peak caused by the initial electron avalanche followed by a delayed peak that moves toward the cathode with an apparent velocity of about twice that of the ions. Steady-state 811-nm emission is also observed in a region of very low electric field near the cathode where the Ar^+ ions have insufficient energy for excitation and the fast atoms are injected from a high-field region. These observations of 811-nm emission, plus previous measurements of steady-state spatial distributions of emission, are interpreted as demonstrating that excitation of the 811-nm lines is primarily by fast Ar atoms formed by charge transfer in $\text{Ar}^+ \text{-Ar}$ collisions. For 750-nm emission the prompt portion is much larger and the delayed portion is much weaker than for 811-nm emission showing the importance of excitation by electrons even at these high E/n values. Steady-state observations of 811-nm emission when slow Ar^+ ions are injected into a region of high electric field further confirm the model.

I. INTRODUCTION

The objective of this research is to demonstrate the importance of excitation of Ar by fast (≈ 100 -eV) Ar atoms or ions. In particular, we wish to test the proposal by Phelps and Jelenković¹ that the source of excitation of the Ar lines near 811 nm at very high ratios of the electric field E to gas density n is excitation of Ar by fast Ar. The experimental techniques chosen were to measure (a) the temporal and spatial dependence of the prebreakdown emission resulting from the passage of a short pulse of photoelectrons through the Ar at the very high E/n values, and (b) the spatial dependence of emission in a known, nonuniform electric field.

Previous measurements of transient prebreakdown behavior in Ar by Molnar,² Varney,³ Kirsch,⁴ and others⁵ have provided data on primary ionization coefficients due to electron impact, secondary-electron yields, and the role of excited metastable states at E/n up to 400 Td. Here $1 \text{ Td} = 10^{-21} \text{ V m}^2$. The present work is primarily concerned with the gas excitation and ionization processes at E/n values from about 400 Td up to 80 kTd. Our transient measurements are made on a short enough time scale such that the effects of metastable atoms produced by electron impact can be neglected.²⁻⁵ Brief summaries of this work have been presented elsewhere.⁶

II. EXPERIMENT

A schematic of the electron drift tube constructed for use at high electric fields and low gas densities is shown

in Fig. 1. Except for the presence of a grid, this is the drift tube and pulsed laser used in measurements⁷ of current growth in N_2 . The 60-mm-diam, semitransparent, AuPd film cathode is illuminated from the back with the quadrupled output (266 nm) of a YAG (yttrium aluminum garnet) laser. The grid was spaced 10 mm from and parallel to the cathode and was constructed of

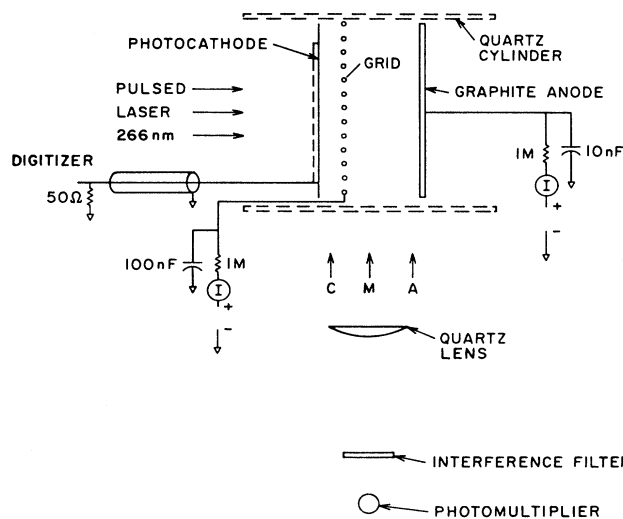


FIG. 1. Schematic of experiment for measurement of temporal and spatial distribution of light output at high E/n .

25- μm stainless-steel wires with an average spacing of 0.25 mm and was measured to be 74% optically transparent. The anode and cathode electrodes are 39 mm apart, 78 mm in a diameter, and provide an approximately spatially uniform field. Except as noted, the grid was operated so as to provide a constant electric field throughout the drift region. An important feature of the drift tube is the very uniform and closely fitting 80-mm internal diameter quartz tube which surrounds the electrodes and prevents long-path breakdown.⁸ The anode was made from sintered graphite. Our previous experiments⁹ showed that the choice of graphite resulted in low yields of reflected electrons at the anode. We have been able to operate the discharge at up to 5600 V between the anode and grid when the cathode was operated at near grid potential to suppress ion- and atom-induced secondary electrons. The corresponding E/n value was approximately 80 kTd.

The magnitude of the transient discharge current is determined by the number of photoelectrons released from the photocathode. Considerable drift of the photocurrent occurred because of variations in the laser output and in the photocathode yield. All data were normalized to the average current. Typically, the average cathode currents were ≈ 20 nA, corresponding to ≈ 0.1 nC per pulse at 20 Hz. The resultant space-charge distortion of the elastic field is small at all except the lowest E/n value used in the nonuniform field experiments. In the steady-state experiments the currents were kept to less than 10 μA by external load resistors so as to limit space-charge distortion. The drift tube current in the transient experiments was recorded with a digitizer having a time resolution of 3 ns. However, the first ≈ 200 ns of the current wave form was usually severely distorted by ringing caused by inductance and shunt capacitance of the leads to the drift tube.

The light emission is observed with a photomultiplier and slit system mounted on a table driven by a computer controlled stepping motor.^{1,9} The letters *C*, *M*, and *A* in Fig. 1 indicate the standard positions of the optical axis when recording transient data and will be referred to as the "near the cathode," "midgap" and "near the anode" positions, respectively. Here, "near an electrode" is taken to be 5 mm from the electrode. The emission was focused into a double-slit system⁹ using a 70-mm-diam quartz achromat lens. For the transient experiment of this paper the slits were relatively open in order to give sufficient signals for the transient measurements. The resultant spatial resolution was about 3.5 mm (full width at half maximum). The steady-state measurements were carried out using the higher-resolution slit settings of Ref. 9, i.e., the resolution was ≈ 1 mm. Interference filters were used to select the wavelengths observed. The photomultiplier had a GaAs(Cs) photocathode with a nearly constant radiant sensitivity 250–820 nm. The photomultiplier output was normally connected to a fast preamplifier and then to the input of the transient digitizer. In some measurements the photomultiplier output passed through a counting chain and was counted by a gated scaler with a variable delay gate.

The vacuum system is all stainless steel with copper

gasket seals except for the quartz windows which use polyurethane O rings. After a bakeout at $\approx 100^\circ\text{C}$ the pressure was 10^{-4} Pa with a rate of rise of 10^{-2} Pa/min. Typical Ar pressures were 4–66 Pa (30–500 mTorr) and the duration of a run was ≈ 10 min. Since the Ar samples were listed by the manufacturer to have fractional impurities of less than 10^{-5} , the principal source of impurities was the background gas. The pressure was measured to $\pm 10^{-2}$ Pa with a diaphragm manometer. Voltage and current were measured with instruments stated to be accurate to $\pm 2\%$. Emission spectra obtained at $E/n \approx 5$ kTd and 100 mTorr in the wavelength range from 200 to 890 nm with a $\frac{1}{4}$ -m monochromator and GaAs(Cs) photomultiplier⁹ showed no evidence of impurities.

The spectral lines used in these experiments are transitions between the $2p$ and $1s$ configurations (Paschen notation¹⁰). A (808 ± 5) -nm filter transmitted the 811.5- ($2p_9 - 1s_5$) and 810.4- ($2p_7 - 1s_4$) nm lines, while 764- and 750-nm filters transmitted the 763.5- ($2p_6 - 1s_3$) and 750.4- ($2p_1 - 1s_2$) nm lines.

III. MODEL OF EXPERIMENT

In this section we extend the model of the collision processes occurring in discharges in Ar at very high E/n and spatially uniform electric fields developed by Phelps, Jelenković, and Pitchford¹¹ to the analysis of the transient results of Sec. IV. In this model the highly non-equilibrium electron motion is approximated using the single-beam approximation,¹¹ while the Ar^+ ions are assumed to be in a local equilibrium at the applied E/n in which the energy gained from the electric field is balanced by the energy loss to the Ar atoms. The fast Ar atoms are assumed to have an initial velocity distribution characteristic of the ions, but to be subject to beamlike attenuation.

A. Complete model

The electron motion will be calculated using the single-beam energy balance model derived and discussed in Sec. II A of Ref. 11. According to this model the rate of spatial and temporal growth of the electron flux density $\Gamma_e(\zeta, t)$ in the space between the electrodes is equal to the sum of the rates of ionization in collisions of electrons, Ar^+ , and fast Ar with Ar. Thus

$$\begin{aligned} \frac{\partial \Gamma_e(\zeta, \tau)}{\partial \tau} + v_e \frac{\partial \Gamma_e(\zeta, \tau)}{\partial \zeta} &= R_i(\zeta, \tau) \\ &\equiv v_e Q_e^i(\varepsilon) \Gamma_e(\zeta, \tau) \\ &\quad + w_p \frac{\alpha_p^i}{n} (E/n) \Gamma_p(\zeta, \tau) \\ &\quad + w_f \frac{\alpha_f^i}{n} (E/n) \Gamma_f(\zeta, \tau). \end{aligned} \quad (1)$$

Here $\zeta = nz$ is the normalized distance or column density measured from the cathode, z is the distance from the cathode, $\tau = nt$ is the normalized time, t is the time from the beginning of the photoelectron pulse, v_e is the veloci-

ty of the electron "beam," $Q_e^i(\varepsilon)$ is the cross section for ionization by electrons of energy ε , w_p is the drift velocity of the ions, $\alpha_p^i(E/n)/n$ is the spatial ionization coefficient for the Ar^+ , $\alpha_f^i(E/n)/n$ is the spatial ionization coefficient for fast neutral atoms, and $\Gamma_p(\zeta)$ and $\Gamma_f(\zeta)$ are the particle flux densities for the Ar^+ and for the fast neutral atoms. The velocity of the fast atoms w_f is defined at the end of this section. The rate of ionizing collisions caused by all processes is $R_i(\zeta, \tau)$. As in previous models,^{1,9,11} the α/n are described as "spatial" reaction or excitation coefficients and are defined as the number of collision events per unit distance in the direction of ion drift. The word "spatial" also distinguishes these coefficients from "temporal" reaction or rate coefficients. A less descriptive terminology sometimes used is "Townsend-type" coefficient, because of their similarity to the "Townsend ionization coefficient." The calculation of these coefficients will be discussed below.

The equation for the spatial and temporal growth of the energy ε of the electron beam includes the energy gain from the field and energy lost in inelastic collisions. Since the model assumes a single energy for all electrons, this equation also includes the energy required to raise the energy of new electrons produced by ionization from essentially zero to the beam energy, i.e.,

$$\frac{\partial \varepsilon(\zeta, \tau)}{\partial \tau} + v_e \frac{\partial \varepsilon}{\partial \zeta} = v_e \frac{eE}{n} - v_e \sum_k \varepsilon_k Q_e^k(\varepsilon) - \varepsilon R_i(\zeta, \tau). \quad (2)$$

Here ε_k and $Q_e^k(\varepsilon)$ are the threshold energy and total cross section for electron excitation for the k th electronic state of Ar. In Eq. (2) we have neglected the loss of energy by electrons in elastic collisions, as is appropriate to the high E/n value of interest.

The continuity equations for the Ar^+ flux density $\Gamma_p(\zeta, \tau)$ and the fast Ar flux density $\Gamma_f(\zeta, \tau)$ in the present model are

$$\frac{\partial \Gamma_p(\zeta, \tau)}{\partial \tau} - w_p \frac{\partial \Gamma_p(\zeta, \tau)}{\partial \zeta} = R_i(\zeta, \tau) \quad (3)$$

and

$$\begin{aligned} \frac{\partial \Gamma_f(\zeta, \tau)}{\partial \tau} - w_f \frac{\partial \Gamma_f(\zeta, \tau)}{\partial \zeta} \\ = w_p Q_{\text{CT}}(\varepsilon) \Gamma_p(\zeta, \tau) - w_f \frac{\alpha_f^a}{n}(E/n) \Gamma_f(\zeta, \tau), \end{aligned} \quad (4)$$

where

$$\frac{\alpha_f^a}{n}(E/n) = \frac{\alpha_f^m}{n}(E/n) + \frac{\alpha_f^i}{n}(E/n) + \frac{\alpha_f^k}{n}(E/n). \quad (5)$$

Equation (3) shows that the increase in the Ar^+ flux density is the result of the same ionizing collisions that produce the increase in the electron flux density. Equations (4) and (5) assume that the growth of fast-atom flux density is the result of charge-transfer collisions of Ar^+ collisions with Ar. In Refs. 11 and 12 it was assumed that the loss of fast atoms occurs by any large-angle scattering collision or energy-loss collision process. More realistic attenuation cross sections will be discussed in Sec. IV B 4. The negative signs on the left-hand sides of Eqs. (3) and

(4) result from the flow of positive ions and, therefore, fast neutral atoms toward the cathode, i.e., toward smaller ζ . In Eq. (4) Q_{CT} is the cross section for charge transfer, α_f^a is the average cross section for the attenuation of fast neutral atoms, α_f^m is the average cross section for momentum transfer in Ar-Ar collisions, and α_f^k is the average cross section for excitation of Ar by the fast Ar in process k .

The boundary conditions to be used with this model are

$$\Gamma_e(0, \tau) = \gamma_p \Gamma_p(0, \tau) + \gamma_f \Gamma_f(0, \tau) + N_0 \delta(\tau), \quad (6)$$

$$\Gamma_p(d, \tau) = \rho \Gamma_e(d, \tau), \quad (7)$$

$$\Gamma_f(d, \tau) = 0, \quad (8)$$

and

$$\varepsilon(0) = 1 \text{ eV}. \quad (9)$$

Here d is the position of the anode, ρ is the yield of ions produced near the anode by low-energy backscattered electrons, N_0 is the number of photoelectrons per unit area produced by the laser, and $\delta(\tau)$ is a delta function at $\tau=0$. We define $(\gamma)_{\text{eff}} = (\gamma_p \Gamma_p + \gamma_f \Gamma_f) / \Gamma_p$. Because of our use of a graphite anode,^{1,9} we will assume $\rho \ll 1$, e.g., 0.05. Although we assume $\varepsilon(0) = 1$ eV, the value is not critical.

The spatial reaction coefficients or average cross sections α_q^x are defined by

$$\begin{aligned} \frac{\alpha_q^x(E/n)}{n} &\equiv \frac{\int dv v Q_q^x(v) f(v)}{\int dv v_z f(v)} \\ &= \frac{1}{kT_+} \int d\varepsilon Q_q^x(\varepsilon) \exp \left[-\frac{\varepsilon}{kT_+} \right], \end{aligned} \quad (10)$$

where q is either p for positive ion or f for fast atom, x is either k for excitation or i for ionization, and $(kT_+)^{-1} \exp(-\varepsilon/kT_+)$ is the normalized steady-state energy distribution for the Ar^+ as given by several authors.¹³ Here v_z is the component of the ion velocity in the direction of the electric field and, because of the one-dimensional velocity distribution, is equal to the ion velocity v . The ion "temperature" T_+ is given¹³ by $kT_+ = eE/(nQ_{\text{CT}})$, and the corresponding drift velocity is $w_p = (2eE/\pi m Q_{\text{CT}})^{1/2}$, where e is the electron charge and k is Boltzmann's constant. Note that the theoretical Ar^+ energy distribution $f(\varepsilon)$ in a one-dimensional distribution, i.e., it is a δ function in directions perpendicular to the electric field and a Maxwellian in the direction of the field. The labeling of α_f^x/n as average cross section is evident from the second form of Eq. (10) and is appropriate only for the one-dimensional energy distribution resulting from charge-transfer collisions. The α_p^x/n are independent of position and are functions of E/n , since kT_+ is a function of E/n . Figures 6–8 and Tables 6–8 of Ref. 12 give values of α_p^x/n used in our model. The average cross sections or spatial ionization coefficients for the fast neutral Ar are also calculated using Eq. (10), since the initial distribution of fast-Ar-atom energies is the same as that for Ar^+ and since the sum of the cross

sections for the attenuation of the fast Ar varies slowly with energy. See Ref. 12.

The model described by Eqs. (1)–(10) does not take into account the distance moved by an excited atom produced in an Ar⁺-Ar or Ar-Ar collision before radiation. This effect is difficult to estimate since we have very little information regarding the velocity and angle of excited atoms after excitation. In Ar-Ar collisions¹⁴ and Ar⁺-Ar collisions¹⁵ the small-angle scattering data show energy losses corresponding to excitation, but information is not available as to the overall importance of this small-angle contribution for low-energy collisions. In H-H₂ excitation collisions, the fraction of fast or “projectile” excited atoms increases with decreasing collision energy.¹⁶ For a fast-atom collision producing an excited atom with an energy of 100 eV and a radiative lifetime of 30 ns, as for the upper level of the 811-nm transition, the distance moved before radiation is less than 1 mm. Excited atoms produced by electron impact move much more slowly and move shorter distances before radiation. Accordingly, we will assume that the excited atoms radiate within a short distance of their point of production. By analogy with the dc emission experiments,^{1,9} it is convenient to express the rate of emission at wavelength λ in terms of an apparent spatial and temporal excitation coefficient given by

$$\frac{\alpha_\lambda(\xi, t)}{n} = \frac{\alpha_p^\lambda}{n} (E/n) \frac{\Gamma_p(\xi, t)}{(N_0/T_i)} + \frac{\alpha_f^\lambda}{n} (E/n) \frac{\Gamma_f(\xi, t)}{(N_0/T_i)} + Q_e^\lambda(\epsilon) A T_i e^{-At} g(z), \quad (11)$$

where T_i is the ion transit time and A is the radiative transition probability for the state emitting at λ . Here we have assumed that the electron current density is given by $\Gamma_e \delta(t) g(z)$, where $\delta(t)$ is a delta function and $g(z)$ is to be determined from the steady-state electron model.^{1,9,11} The approximation is possible because the data of Sec. IV A 1 show that the effective radiative lifetime $1/A$ of the excited Ar is significantly longer than the electron current pulse. Here we have neglected collisional quenching¹ because of the low gas densities at the higher E/n value where the present model holds.

A final aspect of the model is the choice of the fast-atom velocity w_f . The choice is based on the remark by Chantry¹⁷ that the reason the fast atoms appear to move faster than the ions which produced them in charge-transfer collisions is that we observe excitation primarily

by those higher velocity atoms for which the excitation cross section is large. We take w_f as the velocity of those atoms with energies at the peak of the integrand of Eq. (10). For example, at $E/n = 20$ kTd this procedure gives $w_f = 2.3 \times 10^4$ m/s compared to the Ar⁺ drift velocity of $w_p = 8.5 \times 10^3$ m/s. The velocities at which the integrand is one-half of its peak value are approximately 75% and 130% of w_f , so that a significant spreading of the structure of the 811-nm emission wave form calculated using Eq. (11) is expected.

B. Simplified, analytic model

Rather than solve the full set of Eqs. (1)–(11) numerically, we will give approximate analytic solutions which show the essential features of the transient emission observed for excitation by electrons, Ar⁺, and Ar at the very high E/n value of the present experiments. We first note that the electron drift velocities w_e are^{18,19} from 3000 to 10 000 larger than those for Ar⁺ in Ar,¹² so that the steady-state solutions of Eqs. (1) and (2) for the electrons are adequate for emission data obtained on the time scale of the transit of ions and fast neutral atoms between the electrodes. Second, for $E/n < 20$ kTd and voltages well below breakdown, we can neglect heavy-particle ionization terms²⁰ in Eqs. (1) and (3). This assumption needs further investigation for higher E/n and values of nd near, but below, breakdown. Third, since we will apply the model only to experiments for which secondary avalanches are small, we neglect the secondary electrons produced at the cathode, i.e., the model considers only the ions generated in the avalanche initiated by the photoelectrons. Finally, we find that the solution to Eqs. (1) and (2) can be approximated by the empirical relation $\Gamma_e(z, t) = N_0 \delta(t) \exp(\alpha z)$. Here α is an empirical parameter which is adjusted to fit the experimental data or is obtained by fitting to theoretical solutions for the spatial dependence of the ionization produced by the electrons of the initial avalanche and by electrons backscattered from the anode. For the single avalanche conditions of this model α is negative at high E/n because of the decreasing ionization cross section with increasing electron energy over most of the gap. With these approximations, Eqs. (3) and (4) have the solutions

$$\Gamma_p(y, t) = w_p \alpha_e^i N_0 \exp^{-\alpha(y - w_p t)} [1 - u(t - y/w_p)] \quad (12)$$

and

$$\Gamma_f(y, t) = \frac{w_f w_p Q_{CT} n \alpha_e^i N_0}{[\alpha(w_f - w_p) - \beta]} [e^{-\alpha y} (e^{\alpha w_f t} - e^{\alpha w_p t}) u(t) + (1 - e^{\alpha w_f (t - y/w_f)}) u(t - y/w_f) + (1 - e^{\alpha w_p (t - y/w_p)}) u(t - y/w_p)]. \quad (13)$$

Here $y = d - z$ is the distance from the anode, d is the electrode separation, $\beta = w_f \alpha_f^a$, and $u(t - c)$ is the unit step function beginning at $t = c$. The ionization coefficient α_e^i is the maximum value of $v_e(z) Q_e^i(z)$ in gap, i.e., the ionization frequency per molecule at an electron energy of about 100 eV.

The ion current measured at the cathode is determined from the flux of Ar⁺ in the region between the cathode and the grid using the relation

$$J_p = \frac{e}{d} \int_0^{d/4} dz \Gamma_p(z, t) \quad (14)$$

so that

$$J_p = \begin{cases} \frac{ew_p A}{d} e^{\alpha(w_p t - 3d/4)} (1 - e^{\alpha d/4}) & \text{for } 0 < t < \frac{3d}{4w_p} \\ \frac{ew_p A}{d} (1 - e^{\alpha(w_p t - d)}) & \text{for } \frac{3d}{4w_p} < t < \frac{d}{w_p} \end{cases}$$

Here it is assumed that the spacing of the grid from the cathode is $\frac{1}{4}$ of the cathode anode spacing as in our experiment.

The predictions of the analytic model are illustrated in Fig. 2, where the calculated current wave form is shown in the upper trace, the calculated emission near the cathode and near the anode are shown in the middle and lower traces. Here we have chosen α to be negative so as to be consistent with the data discussed in Sec. IV A 2 for the lowest Ar densities used. In the lower sections of Fig. 2, the solid curves show the predicted total production of 811-nm emission by electrons, fast Ar atoms, and Ar^+ for a position near the cathode and for a position near the anode. The dash-dotted curves show the predicted excitation by electrons when the excited states are assumed to decay with the lifetime of 200 ns found experimentally in Sec. IV A 1. Also shown by the dashed line in the set of curves for a position near the cathode is the predicted contribution of excitation by Ar^+ multiplied by a factor of 70. The slow rise in the predicted emission at 1–2 μs in Fig. 2 results from the extra collision required for excitation by fast Ar relative to that for excitation by Ar^+ .

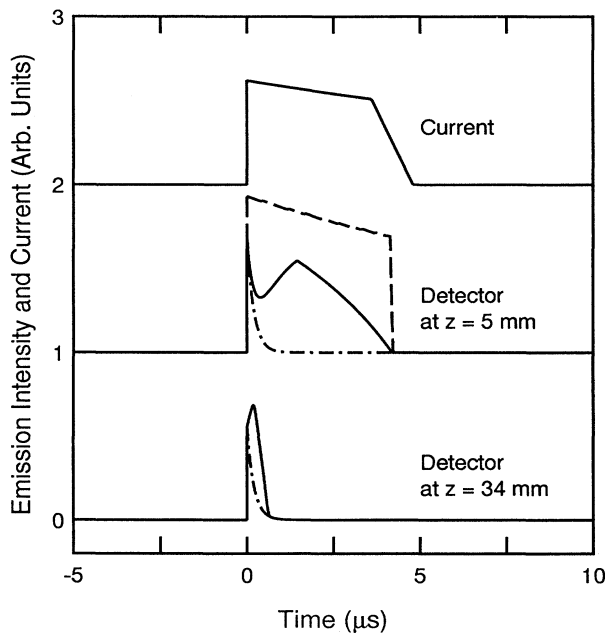


FIG. 2. Calculated cathode current and 811-nm emission wave forms for $E/n = 18.6$ kTd and an Ar density of $9.7 \times 10^{20} \text{ m}^{-3}$ (0.03 Torr). The solid curves show the total emission. The dash-dotted curves show the emission resulting from electron excitation, while the dashed curve shows emission resulting from excitation by Ar^+ after multiplication by 70.

This difference in time dependences is analogous to the difference in spatial dependences predicted and observed for 811-nm emission.¹ Note that since we estimate that the ion nonequilibrium distance is $< 5\%$ of the electrode spacing in the data to be presented, we have not attempted to include the corresponding delay in the models of this section. The results for the simplified model will be compared with experiment in Sec. IV A 2.

IV. RESULTS

A. Uniform electric fields

1. $E/n = 280$ Td data

Measurements of electron-induced ionization²¹ and emission¹ for Ar at $E/n < 1000$ Td show that over most of the gap the electrons are in local equilibrium with the electric field and gas collisions as required for application of the conventional model of current growth.^{5,22} An example of such data is shown in Fig. 3 for $E/n = 280$ Td and an Ar pressure of 0.5 Torr, where 1 Torr = 133 Pa. The upper trace of Fig. 3 shows the electron current, while the lower trace shows the emission from Ar at 811 nm when the detector is located near the anode. The first peak in the current at 200 ns is caused by the laser-induced photoelectron pulse and has a width determined primarily by the transit time of the electrons between the cathode and the grid. The second and much smaller peak at 300–400 ns is apparently caused by photon-induced secondary electrons,^{5,22} where the photons are excited by electrons which have crossed most of the gap. The elec-

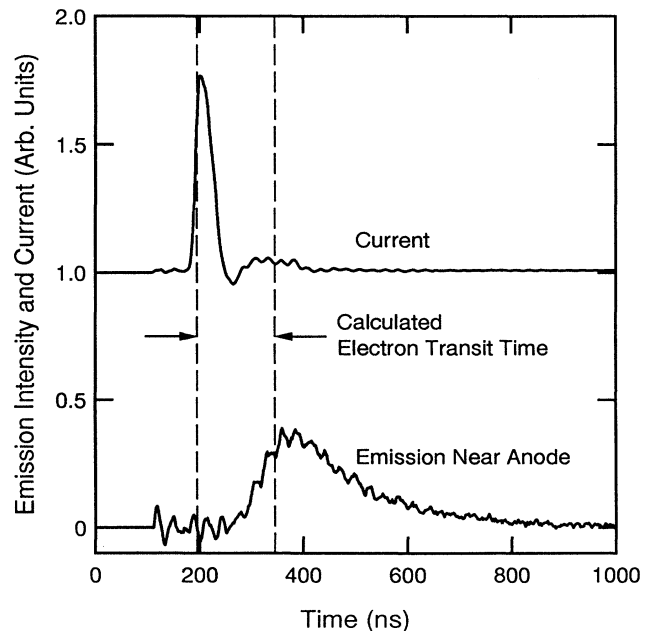


FIG. 3. Cathode current and (811 ± 1) -nm emission transient near anode for $E/n = 280$ Td. The laser-induced photoelectron pulse occurs at 200 ns. The Ar density was $1.6 \times 10^{22} \text{ m}^{-3}$ (0.5 Torr).

tron transit time for crossing the gap calculated using the theoretical drift velocity of Golant¹⁹ is shown by the dashed vertical line. The small negative current signal near 260 ns is probably caused by the damped, ringing-type oscillations observed when the current pulse is short.

The time of maximum rate of increase in the 811-nm emission near the anode in Fig. 3 corresponds approximately to the estimated electron transit time. In the time interval from 200 to 1000 ns the 811-nm emission decays with a time constant of 150 ± 20 ns compared to the ≈ 30 -ns radiative lifetimes¹⁰ for the upper levels of the 811-nm transitions. This slow decay has been attributed by Gallagher²³ to cascading from states of the $3d$ and $1s$ configurations (Paschen notation¹⁰) that are efficiently excited by high electron energy electrons. Similarly long decay times have been observed by Cooper *et al.*²⁴ using 0.5-MeV electron-beam excitation and are attributed to cascade excitation. Because of the repeated absorption and emission (imprisonment) of the uv radiation,²⁵ the effective lifetimes of the resonance states of the $3d$ configuration approach the lifetimes for the $3d$ to $2p$ transitions, i.e., about 100 ns.¹⁰ In this explanation the photons responsible for the secondary-electron emission at the cathode at our lower E/n are presumably from the $3d$ - $1p$ transitions near 87 nm, rather than from the $1s$ - $1p$ transitions near 105 nm that are usually considered. Note the relative absence of a significant component of the 811-nm emission near 200 ns corresponding to $2p_9$ or $2p_7$ atoms excited by the initial electron avalanche and decaying with the short radiative lifetimes (≈ 30 ns) characteristic of $2p$ states.¹⁰ Experimental excitation cross section data are available²⁶ for the $2s$ and $3d$ levels only for energies up to 100 eV. Qualitative evidence for large excitation cross sections for the $3d$ levels at 400 and 500 eV is given by Li *et al.*²⁷ Several estimates of these cross sections have been made using optical oscillator strength data.²⁸

Note that the long-lived $2s$ and $3d$ excited states responsible for the cascade excitation of the $2p$ levels following electron excitation of Ar will have short radiative lifetimes, i.e., 3–30 ns,¹⁰ when the $2s$ and $3d$ levels are produced with significant velocities in Ar-Ar or Ar⁺-Ar collisions and imprisonment effects²⁵ are small. We therefore expect cascade excitation of the $2p$ levels from the $2s$ and $3d$ levels to be small following excitation of the $2s$ and $3d$ levels in Ar-Ar and Ar⁺-Ar collisions.

2. $E/n = 18.6$ kTd data

The results of time-dependent measurements of 811-nm emission and discharge current for $E/n = 18.6$ kTd are shown in Figs. 4 and 5 for Ar pressures of 30 and 50 mTorr, respectively. The total discharge voltages vary from $V = 720$ to 1200 V. Since the corresponding mean free paths of 2.5–1.4 mm for the Ar⁺ are short compared to the 40-mm gap, we assume the Ar⁺ to be in equilibrium with the applied E/n and to have the calculated^{1,13} energy distribution with $kT_+ = 47$ eV. The current transient shown by the solid curve in the upper trace of Fig. 4 is severely distorted at early times, e.g., less than ≈ 100 ns, because the short (≈ 30 ns) electron

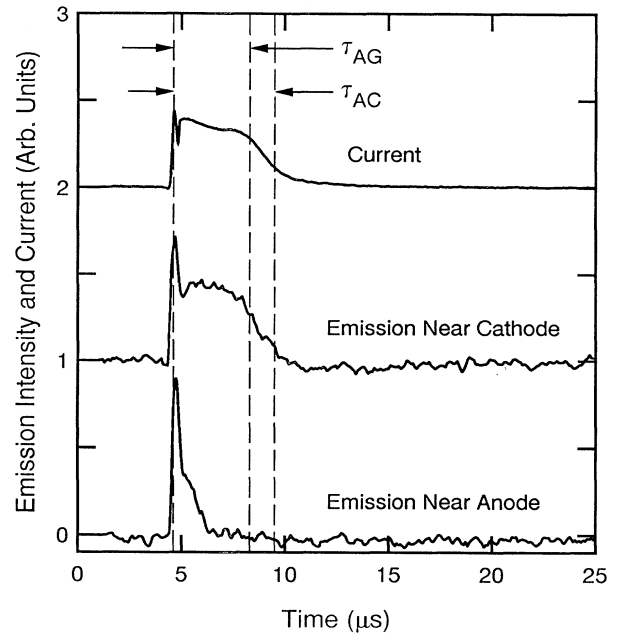


FIG. 4. Cathode current and (811 ± 1) -nm emission transients following a laser pulse at $4.5 \mu\text{s}$ for $E/n = 18.6$ kTd at various positions. The Ar density was $9.7 \times 10^{20} \text{ m}^{-3}$ (0.03 Torr). The calculated ion transit times are τ_{AG} and τ_{AC} for the anode to grid and anode to cathode, respectively.

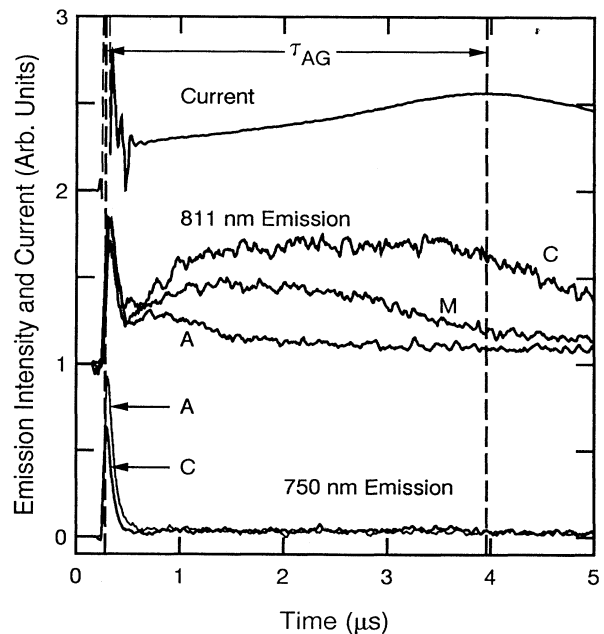


FIG. 5. Cathode current, 811 ± 1 nm, and 750.4-nm emission transients following a laser pulse at $0.3 \mu\text{s}$ for $E/n = 18.6$ kTd at various positions. The Ar density was $1.6 \times 10^{21} \text{ m}^{-3}$ (0.5 Torr). The time τ_{AG} is the calculated anode-grid ion transit time. The traces marked C, M, and A are for positions near the cathode, at midgap, and near the anode, respectively.

current pulse is not recorded by the transient digitizer when operated at slow sweep speeds ($> 5 \mu\text{s}/\text{cm}$). Current traces recorded at higher sweep speeds are not useful because of the presence of damped circuit oscillations as is shown in Fig. 5. The remainder of the current wave forms in Figs. 4 and 5 are proportional to the average flux of delayed ions and electrons between the grid and the cathode as given by Eq. (14). The calculated ion transit times from the anode to the grid τ_{AG} and from the anode to the cathode τ_{AC} are indicated by the vertical dashed lines. The reproducible minimum in the current in Fig. 4 near $5 \mu\text{s}$, i.e., just after the electron current spike, may be evidence for ion nonequilibrium effects, but also could be residual circuit oscillations. The relatively slow decrease in current between 5 and $8 \mu\text{s}$ in Fig. 4 is caused by the arrival of a decreasing ion flux, resulting from the decrease in ion production with distance from the cathode as the electrons gain energy.^{1,9,11} The small structure in this current wave form occurring just prior to the calculated ion transit time τ_{AG} is probably caused by additional ions produced near the anode by backscattered electrons.

A second important feature of the current wave form in Fig. 4 is the small magnitude of the current flowing after collection of the Ar^+ from the initial avalanche, i.e., after τ_{AC} . The small area under this portion of the current wave form means that the ionization and excitation caused by secondary avalanches can be neglected, as is assumed in the model of Sec. III B. The very low emission from near the anode at times from 7 to $9 \mu\text{s}$ is also evidence for the negligible contribution of secondary avalanches to the emission.

The wave form in the middle trace of Fig. 4 is the 811-nm emission 5 mm from the cathode. The initial peak at $5 \mu\text{s}$ is the result of the production of $2p$ atoms by the photoelectrons and by electrons produced in the initial avalanche. The second and broader emission maximum, lasting from 5 to $10 \mu\text{s}$, will be referred to as delayed emission. Most of this emission is produced by a "wave" of particles which move toward the cathode with velocities that are slow compared to electron velocities. Evidence for this wavelike motion is the much earlier decrease in the delayed emission when observed at a position near the anode, as in the lower trace of Fig. 4. Similar wavelike behavior, but for a higher Ar density, is seen in the upper and middle traces of Fig. 5. Since the excited states responsible for the production of 811-nm radiation have a radiative lifetime of less than 200 ns, these atoms emit near where they were excited and must have been excited by some slow-moving species in the wave. From the microsecond time scale of the moving species, we conclude that the particles are either Ar^+ or fast Ar produced by Ar^+ in charge-transfer collisions with Ar. If electrons from secondary avalanches were responsible for the excitation, the 811-nm emission would be independent of the position of observation.

We next use the comparison of the wave forms of Fig. 4 with model predictions shown in Fig. 2 to argue that the dominant excitation is by fast Ar atoms. This argument is based in part on the slow rise in the emission predicted in Fig. 2 to occur immediately after the electron

spike for a detector located near the cathode. The trace labeled C in the middle panel of Fig. 5 shows this rise particularly well. A second part of the argument is concerned with the somewhat more rapid decrease in the emission intensity than in the current observed in the middle and upper traces of Fig. 4. The more rapid decay of emission relative to current is much less pronounced in Fig. 4 than in the middle and upper calculated traces of Fig. 2 because of the spread of fast-atom velocities not included in the model. In both Figs. 4 and 5 the experimental emission wave forms near the cathode are very different from that predicted for excitation by Ar^+ as shown by the dashed line in the middle section of Fig. 2. We have not attempted a quantitative comparison of theory with experimental wave forms because of the distortion introduced by the absorption of ion and fast atoms by the grid.

We conclude from these comparisons of experiment and the model that our observations are consistent with the proposal¹ that excitation by fast atoms is the dominant source of excitation of 811-nm emission at high E/n values. Obviously, a more complete model is very desirable. Further experimental evidence for excitation by fast atoms will be cited in later sections.

The temporal behavior of the 750-nm emission from the $2p_1-1s_2$ transition, shown in lower traces of Fig. 5, is very different from that of the 811-nm emission shown in the middle traces. Following the initial spike caused by electron excitation during the initial avalanche, there is a weak, slowly varying emission lasting for times about equal to the ion transit time. The signal-to-noise ratio is not high enough to say whether the time dependence of this delayed 750-nm emission follows the 811-nm emission produced by fast Ar or the expected secondary electron flux resulting from Ar^+ arriving at the cathode. The relatively large initial spike on the time scale of the initial electron avalanche and the weak delayed emission are consistent with excitation of the 750-nm lines by electrons. A large probability of electron excitation of 750 nm compared to 811 nm is expected since Ballou, Lin, and Fajen²⁹ have shown that the cross section for electron excitation of the $2p_1$ level and the 750-nm line of Ar is ≈ 25 times that for the $2p_9$ level and the 811.5-nm line at 200 eV and that the ratio increases with increasing electron energy. In addition, Kempter *et al.*³⁰ found that the cross section for the excitation of the 750-nm lines in fast Ar-Ar collisions at 900 eV is only about 20% of that for excitation of the 811-nm lines. This suggests a large cross-section ratio for 811 to 750-nm excitation at the fast Ar energies of our experiment of ≈ 45 eV. Additional discussion concerning the mechanism of 750-nm production will be presented in Sec. IV B 3.

The effects of increasing Ar density at $E/n = 18.6$ kTd are seen by comparing the wave forms of Figs. 4 for 30 mTorr and 5 for 50 mTorr. Most noticeable is the increase with pressure in the slope of the current wave form during the time period τ_{AG} . The negative slope at the low Ar densities of Fig. 4 is partly the result of the decrease in the ionization cross section as the electrons are accelerated in their essentially free-fall motion and partly the result of ion losses to the grid. As the gas density in-

creases the ion current increases and the contribution of secondary avalanches to the current increases. The secondary avalanches are evident in a slower decline in current at the end of τ_{AG} for the conditions of Fig. 5 compared to the decline seen in Fig. 4.

3. $E/n = 52$ kTd data

The current and 811-nm emission wave forms obtained for $E/n = 52$ kTd and a pressure of 30 mTorr are shown in Fig. 6. There are several important differences from the results obtained for $E/n = 18.6$ kTd. First, the electron components of the emission wave forms relative to the delayed components are factors of 2–3 smaller at $E/n = 52$ kTd because of the lower cross sections for direct and cascade excitation by electrons at the higher energies. Second, the time scale of the delayed emission is approximately a factor of 2 shorter than for the 18.6-kTd data. The agreement of the predicted anode to grid transit time τ_{AG} and the measured time to maximum current can be regarded as a test of the assumption that the Ar^+ ions are in equilibrium at this extremely high E/n value. Finally, when the time scales are normalized to the ion transit time, the delayed 811-nm emission wave forms rise more slowly than is the case for 18.6 kTd. This feature suggests that the ratio of atom velocity for maximum excitation probability defined in Sec. III B to the ion velocity for 52 kTd is smaller than for 18.6 kTd. The theory is not sufficiently well developed to test the predicted 25% reduction in w_f/w_p for 52 kTd compared to that for 18.6 kTd.

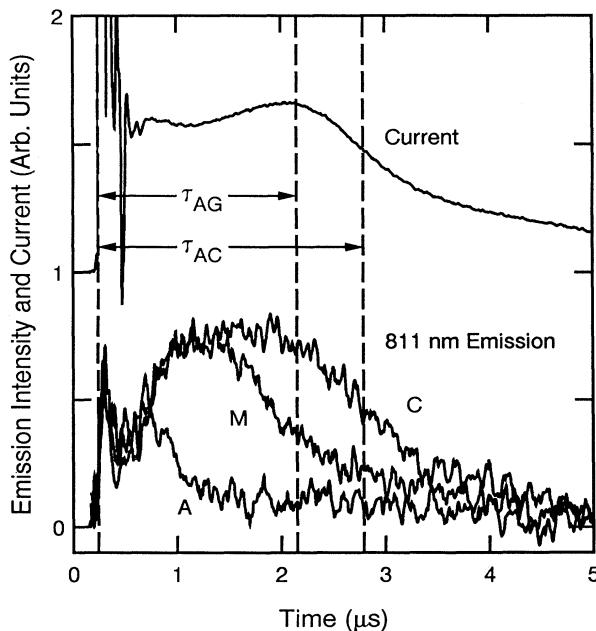


FIG. 6. Cathode current and (811 ± 1) -nm emission transients for $E/n = 52$ kTd at various positions. The Ar density was $9.7 \times 10^{20} \text{ m}^{-3}$ (0.03 Torr). The times and positions indicated are as for Figs. 4 and 5.

B. Nonuniform electric fields

The grid shown in Fig. 1 was added so as to allow the operation of the region between the grid and the cathode at various electric fields relative to that between the anode and grid. Two electric-field configurations for which we will present results are shown schematically in Fig. 7. In the nonuniform field configuration shown in Fig. 7(a) we expect the drift energy of the ions in the cathode-grid region to drop to a few eV and the production of fast atoms with sufficient energy for excitation to cease. The fast atoms passing through the grid have a long enough mean free path so that a significant fraction reach the cathode without collision. The uniform field configuration shown in Fig. 7(b) is the same as that used for the data reported in Figs. 4 and 5. Experiments with nonuniform electric fields were carried out to determine (a) the transient current and emission, (b) the spatial dependence of electron-induced emission and of delayed excitation produced primarily by fast atoms, and (c) the spatial dependence of emission from a steady-state, nonuniform field discharge.

1. Transient currents and emission

The wave forms in Fig. 8(a) show the currents and the 811-nm emission obtained using the spatially nonuniform electric field of Fig. 7(a), while those in Fig. 8(b) were obtained with the spatially uniform electric field of Fig. 7(b). In particular, the voltages between the grid and anode were the same for the two configurations, while the grid-to-cathode voltage for the wave forms on the left was lower by a factor of 18. The current and emission wave forms for the uniform field case in Fig. 7(b) are the same as those of Fig. 4. The general features of these wave forms were discussed in Sec. IV A 2.

The initial peak in the current wave form for the nonuniform field case is caused by the photoelectron pulse. This pulse is recorded by the digitizer because of the relatively low electron drift velocity at $E/n = 1$ kTd and the relatively long times spent by the electrons in the cathode-grid region. The remainder of the current wave form is caused primarily by ions. The calculated ion

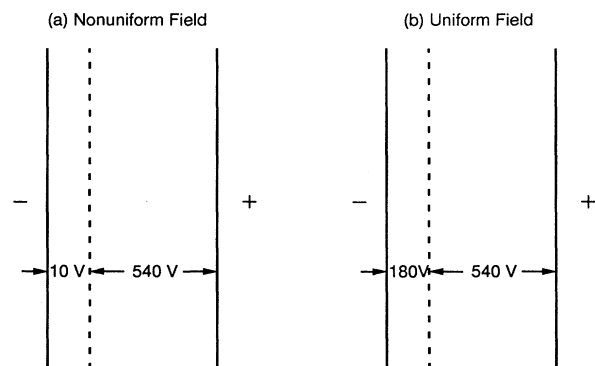


FIG. 7. Schematic of potentials applied in (a) nonuniform field and (b) uniform field experiments of Figs. 8 and 9.

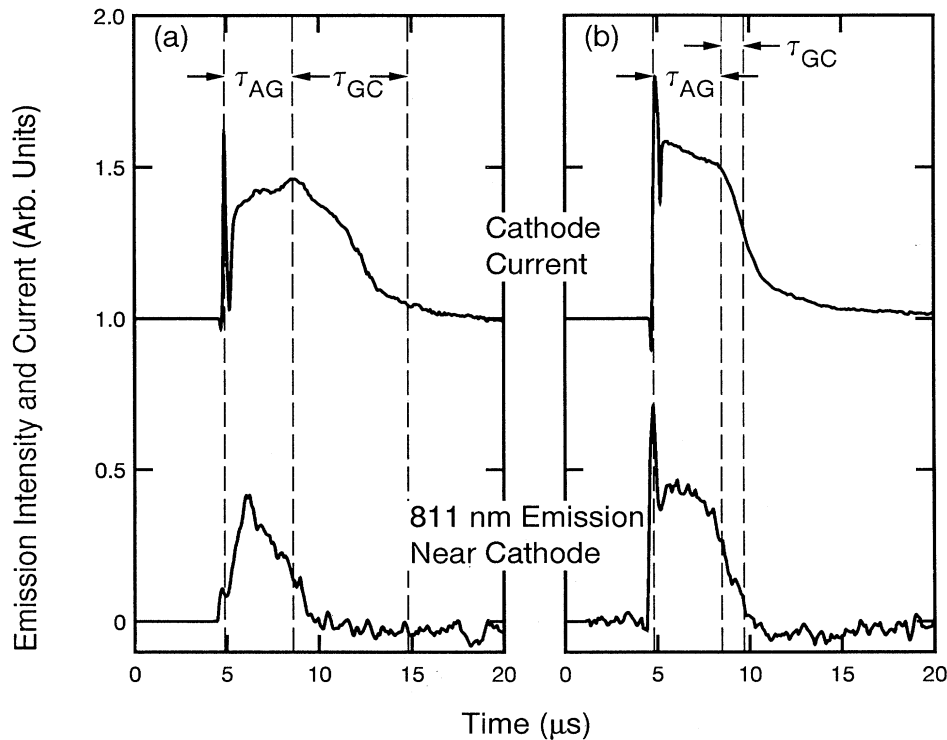


FIG. 8. Cathode current and (811 ± 1) -nm emission transients following a laser pulse at $\approx 4.8 \mu\text{s}$ for nonuniform and uniform electric fields with voltages as shown in Fig. 7. The E/n value between the grid and anode was 18.6 kTd . (a) In the nonuniform field case the E/n value was 1.03 kTd between the cathode and grid. (b) In the uniform field case the E/n value in the grid to cathode region was 18.6 kTd . The calculated ion transit times are τ_{AG} and τ_{GC} for the anode to grid and grid to cathode, respectively. The Ar density was $9.7 \times 10^{20} \text{ m}^{-3}$ (0.03 Torr).

transit times are indicated by τ_{AG} for the anode-to-grid gap and τ_{GC} for the grid-to-cathode gap. The stretched-out appearance of the current wave form after about $8 \mu\text{s}$ is the result of the factor of $\sqrt{18}$ times longer ion transit time across the grid-to-cathode region than in the uniform field case. Thus the “tail” of the wave form is approximately four times longer than for the uniform field case.

The lower wave form of Fig. 8(a) shows the 811-nm emission for the nonuniform field case. Because of the low energy of the electrons in the cathode-grid region there should be no excitation and the small prompt emission peak must be stray light from elsewhere in the drift tube. The relatively sharp peak of the delayed 811-nm emission near $6 \mu\text{s}$ is similar to that shown in Fig. 2 for monoenergetic Ar. It may indicate a relative deficiency of lower energy Ar because of their more rapid attenuation and the absence of production in the low E/n region. In any case, the time-integrated magnitude of the delayed 811-nm signal is reduced by only about 30% from that for the uniform electric field signal of Fig. 8(b). This small change is consistent with the reduced production region for fast Ar and is consistent with excitation by fast Ar. If ions were responsible for the excitation we would expect a drastic reduction in the 811-nm emission because the low E/n value in the grid-cathode region lowers T_+ by a factor of 18, i.e., to values well below the excitation threshold, in about one ion mean free path.

2. Spatial and temporal dependence of 811-nm emission

The second type of experiment carried out using the nonuniform electric-field configuration was the determination of the spatial distribution of the emission using the movable optical and photomultiplier system described previously.^{1,9} A significant difference from previous experiments was the use of a gated scaler to sample the photomultiplier output and allow measurements of the spatial distribution of emission during the electron pulse or during the later portions of the emission wave form. Figure 9 shows the results of these measurements for the same voltages and pressures as in Fig. 8. The open points were obtained using the nonuniform electric field as in Figs. 7(a) and 8(a), while the solid points were obtained with the uniform electric field as in Figs. 7(b) and 8(b). The square points were obtained by gating the detection system so as to count photon pulses only during a 500-ns period centered on the emission caused by the initial electron avalanche, while the circular points were obtained during a 5- μs period beginning $0.5 \mu\text{s}$ after the electron-induced signal. All measurements are normalized to the average cathode current.

The excitation produced during the initial electron avalanche for the uniform electric field case, i.e., the solid squares, show little variation with position over most of the gap. The nearly spatial-independent excitation produced by electrons is unexpected in view of slowly de-

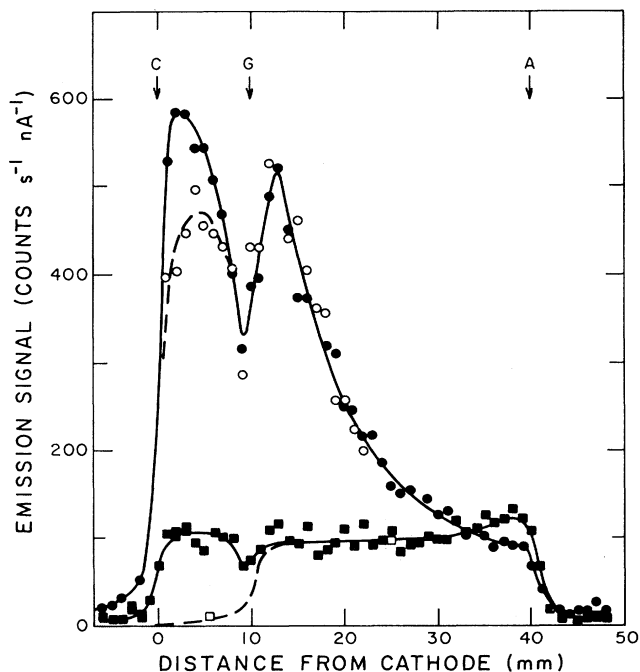


FIG. 9. Spatial dependence of (811 ± 1) -nm emission for the conditions of Figs. 7 and 8. The solid and open squares are from counts arriving during a $0.5\text{-}\mu\text{s}$ gate that includes the initial laser pulse. The solid and open circles are for a $5\text{-}\mu\text{s}$ gate beginning $0.5\text{ }\mu\text{s}$ after laser pulse. The solid points are for the uniform electric field and the open points are for the nonuniform electric field. The voltages were as shown in Fig. 7.

creasing current wave forms of Figs. 4 and 8(b) at the same pressure. The low points at 10 mm from the cathode are attributed to the scattering and/or absorption of the 811-nm photons by the grid. The near equality of the electron-induced emission in the grid-anode and cathode-grid regions suggests that the loss of electrons to the grid is compensated by ionization produced by backscattered electrons from the grid and/or that the resultant electron-energy distribution contains a larger fraction of low-energy electrons capable of exciting the 811 nm efficiently. Backscattering from stainless steel is known to be large and to lower the electron energy.^{9,11} The slight rise in the emission at 35–38 mm from the cathode is attributed to excitation by backscattered electrons from the graphite anode.^{1,9,11}

In the case of electron-induced excitation in the nonuniform field case, gated scaler data were not taken. However, the relative magnitudes of initial peaks of emission transients such as shown in Figs. 4 and 5 were measured. These data, indicated by the open squares in Fig. 9, show that the emission drops by about a factor of 5 from the high-field, grid-anode region to the low-field, cathode-grid region. Since the 10 eV energy available to electrons at the grid is well below the excitation threshold for the 811-nm lines, we suspect that the small signal observed at 5 mm from the cathode is due to scattered light or to the

finite spatial resolution (≈ 3.5 mm) of the detection optics used in the experiments.

The delayed emission from the grid-anode region in Fig. 9 is typical of the spatial dependence observed and calculated¹ for excitation by fast Ar atoms. When normalized to the total anode current, it changes little as the electric field in the cathode-grid region is lowered from the uniform electric field (solid circles) to the nonuniform field (open circles). This insensitivity to the cathode-grid region conditions results from the fact that the flux of ions and fast atoms is zero at the anode and the production of ions is fixed by the normalization to total anode current. A surprising feature of the delayed emission in the uniform electric field case is the relatively large signal in the vicinity of the anode. This emission may be caused by electrons from secondary avalanches,^{1,3} although the small 811-nm emission at $7\text{--}8\text{ }\mu\text{s}$ in the lowest trace of Fig. 4 shows such avalanches to be small for the conditions of Fig. 4. If secondary avalanches are significant because of changed electrode condition, etc., then the $5\text{-}\mu\text{s}$ gate length applied to the scaler was too short. This would result in a discrimination against late time emission, such as occurs predominantly near the cathode. See Figs. 4 and 5. Errors in the settings of the gates are believed to be small.³¹

From the data of Fig. 9, we see that the perturbation of the delayed emission caused by the grid is severe in the uniform field case even if we disregard the emission from within the $\approx 5\text{-mm}$ region obscured by the grid support and apparatus resolution. In view of the measured 74% optical transmission of the grid and the large ratio fast-atom mean free path to grid thickness in the field direction, we expect the excitation by fast atoms to be about 25% smaller than that predicted by extrapolation of the emission observed in the grid-anode region toward the cathode. The observed decrease in emission in the grid-cathode region would seem to be somewhat larger than predicted. The loss of ions at the grid is difficult to estimate because of the sensitivity of the ion motion to the local electric field. Some comments on this point are given in the Appendix.

The delayed excitation in the space between the cathode and grid is reduced in the low-field case compared to the uniform field case because the Ar^+ drifting toward the cathode loss excess energy in about 1 mm in charge-transfer collisions and no longer have sufficient drift energy to produce the fast Ar that cause excitation. The difference in excitation between the uniform and nonuniform field cases in Fig. 9 increases as one approaches the cathode because of attenuation of the fast-atom flux and the absence of fast-atom production in this region. See Sec. IV B 4.

The spatial variations of the sums of the electron and delayed emission components of the 811-nm emission from the grid-anode region for both the uniform and nonuniform field cases shown in Fig. 9 for $E/n = 18.6$ kTd are similar to the spatial dependence of steady-state emission for $E/n = 22$ kTd shown in Fig. 9 of Ref. 1. As suggested in Ref. 1 and discussed in Sec. IV B 4, the 811-nm emission near the anode appears to be due to the contribution of 811-nm excitation by cascading from the

higher resonance levels excited by high-energy electrons.

From the preceding analyses of the spatial-dependence emission data of Fig. 9, we conclude that in the nonuniform field case the excitation in the grid-cathode region is primarily the result of fast atoms injected into the low-field region from the high-field region.

3. Spatial and temporal dependence of 764- and 750-nm emission

Measurements were also made of the spatial dependences of the electron and delayed components of emission at 763.5- ($2p_6-1s_5$) and 750.4- ($2p_1-1s_2$) nm. For the uniform field configuration, the spatial variation of the electron component at both wavelengths was very similar to that shown by the solid squares of Fig. 9. The count rates for the electron components were in the ratios of 6:4:1 for the 750, 811, and 764 nm signals. The delayed 764-nm emission showed much the same spatial variation as the 811-nm emission in Fig. 9, but was a factor of 5 smaller. The delayed 750-nm emission, however, increased by only about 50% in going from the anode to cathode and is much less perturbed by the grid than for the 811-nm lines. This observation is consistent with fast Ar excitation of the 750-nm line equaling about 50% of the electron excitation near the cathode and less than 10% of the electron excitation near the anode. In view of these numbers we conclude that the 750-nm emission from near the anode can be used as a measure of the electron transient behavior in somewhat the same way as the 391.4-nm band emission is used^{7,9} for monitoring the electron transient and spatial behavior in N_2 discharges at very high E/n values.

4. Steady-state measurements of 811-nm emission

Figure 10 shows examples of steady-state emission at 811 nm obtained with various spatially nonuniform electric-field configurations. In these plots, as well as others in this paper, the ions and fast atoms move from right to left and the electrons left to right. Figures 10(a) and 10(b) are for the injection of moderate- and high-energy atoms from the anode-grid region into the zero-field grid-cathode region. Figure 10(c) shows the results of the injection of relatively low-energy ions into a high-electric-field grid-cathode region where the ion drift energy is high enough to produce fast atoms which excite 811-nm emission. Because of the higher spatial resolution (≈ 1 mm) and resultant limited extent of the grid perturbation for the data of Fig. 10, we can obtain much more information regarding the spatial dependence of emission in the grid-cathode region from Fig. 10 than from the data of Fig. 9.

When considering the nonuniform field cases we have used two classes of fast-atom beams. The first is formed by Ar^+ -Ar charge-transfer collisions in the anode-grid region and has an energy distribution characteristic of ions with the anode-grid E/n . The second fast atom beam is formed in the grid-cathode region and has an energy distribution characteristic of ions with the grid-cathode region E/n . Because of the short mean free path

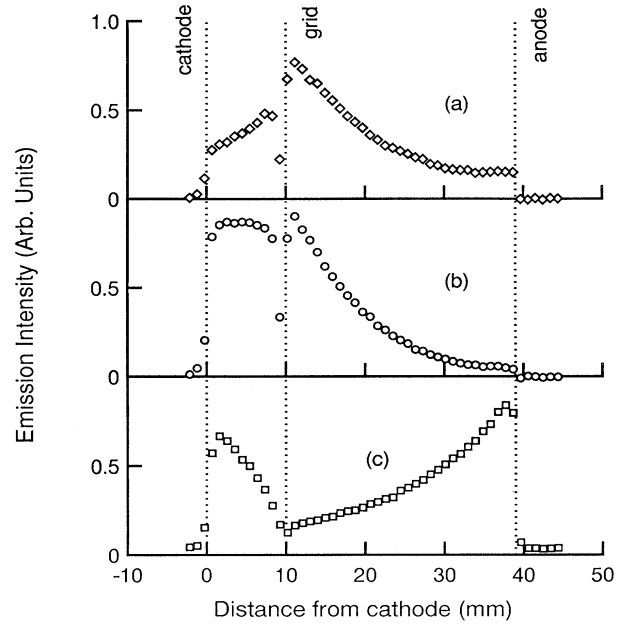


FIG. 10. Experimental spatial dependences of (811 ± 1) -nm emission from steady-state discharges in various nonuniform electric-field configurations. (a) $E/n|_{AG}=14.7$ kTd, $E/n|_{GC}=0$, and $p=80$ mTorr; (b) $E/n|_{AG}=84$ kTd, $E/n|_{GC}=0$, and $p=50$ mTorr; (c) $E/n|_{AG}=2.5$ kTd, $E/n|_{GC}=15$ kTd, and $p=80$ mTorr. In (a) and (b) fast Ar atoms with effective energies of 100 and 300 eV are injected into the electric-field-free grid-cathode region. In (c) slow Ar^+ ions are injected into the grid-cathode region where they rapidly acquire sufficient drift energy to produce the fast Ar atoms, which excite the 811-nm emission.

for charge transfer the ions are assumed to have an energy distribution determined by the local E/n .

The E/n value of 14.7 kTd in the anode-grid region of Fig. 10(a) produces a calculated kT_+ of 36 eV for the injected ions and fast atoms. According to the model of Sec. III, the energy of the fast atoms most responsible for excitation of the 811-nm emission is ≈ 100 eV. Once the ions enter the low-field region they thermalize in about 1 mm and are collected by the grid. The high efficiency of ion collection is evidenced by the very low cathode current, i.e., $\approx 0.1\%$ of the anode current. After passing through the grid with a 25% loss of intensity, the fast atoms continue toward the cathode as a beam while energy loss in $\approx 90^\circ$ angle scattering collisions reduces the directed atom flux, i.e., attenuates the beam. From the decrease in 811-nm intensity with distance to the left of the grid we find an attenuation cross section of $\approx 4 \times 10^{-20}$ m². Note that since 180° elastic scattering in the center-of-mass coordinates results in no loss of fast Ar flux, this attenuation cross section is closely related to the viscosity cross section appearing in thermal conductivity.³² Our attenuation cross section is in good agreement with the viscosity cross section of Robinson³³ of 3.2×10^{-20} m² at 100 eV.

Incidentally, the steady-state model of Ref. 1 shows

that for the conditions of Fig. 10(a) the fast atoms in the grid-cathode region produce sufficient ionization to maintain the discharge without a significant production of secondary electrons from the cathode. The maximum in the 811-nm emission to the right of the grid is caused in part by secondary electrons produced at the grid which are then accelerated through the energy region of maximum cross section. Note that the conditions of Fig. 10(a) are very similar to those in Fig. 9.

The E/n value of 84 kTd in the anode-grid region for Fig. 10(b) produces a calculated kT_+ of 230 eV for the injected ions and fast atoms, so that the atoms that are most effective for excitation have energies of ≈ 300 eV. In this case the cathode current is about 1% of the anode current, again indicating that most ions are collected by the grid and that ionization in the cathode grid region is small. Again, there is a significant loss of fast atoms and ions when transversing the grid. The apparent attenuation cross section for the fast atoms is $< 6 \times 10^{-21}$ m², which is considerably smaller than our previous estimate^{1,13} based on the sum of the cross sections for momentum transfer and inelastic collisions. The probability of excitation by fast atoms is insensitive to energy-loss collisions at this relatively high atom energy because of the slow variation in the excitation cross section with energy. On the other hand, scattering at angles of $\approx 90^\circ$ should still attenuate the beamlike character of the fast atoms. We have no explanation for this apparent attenuation cross section being significantly smaller than Robinson's³³ viscosity cross section of 2×10^{-20} m².

It should be noted that for the conditions of Fig. 10(b) the 811-nm emission increases with very nearly an exponential dependence on distance from the anode toward the grid. From our model calculations,¹ this observation should not be considered as evidence for excitation as the result of an "ion and fast-atom avalanche," but instead is the result of a combination of fast-atom excitation over much of the anode-grid region and of electron excitation toward the anode. In order for a true ion-fast-atom avalanche to develop, the length of the region of observation would have to be long compared to the fast-atom mean free path.

The data shown in Fig. 10(c) are for an E/n value of 2.2 kTd in the anode-grid region and 15 kTd in the grid-cathode region. At the low E/n value of the anode-grid region the ion energy is only $kT_+ = 4.2$ eV so that ionization and cascade excitation are dominated by electrons with energies of about 100 eV energy. The ion flux generated in the anode-grid region drifts through the grid to the high E/n region between the grid and cathode. There the Ar⁺ ions rapidly reach an equilibrium kT_+ of 35 eV and produce a flux of fast Ar that increases toward the cathode. In the grid-cathode region the fast atoms most effective in producing excitation have energies of ≈ 100 eV. Note that the fast-ion flux in the grid-cathode region is formed from the slow-ion flux in about one mean free path, i.e., 1 mm, from the grid. This results in a spatial growth of the fast-atom flux and the resultant 811-nm excitation which is approximately a linear function of distance from the grid toward the cathode. The departures from linearity may be in part caused by sha-

dowing by the grid support. This approximately linear behavior is to be contrasted with the situation near the anode in Figs. 10(a) and 10(b) where we expect¹ the growth of ion flux to be a linear function of distance from the anode and the flux of fast atoms and the excitation to increase quadratically with distance. If the excitation of 811-nm emission by ions in the grid-cathode region for Fig. 10(c) were significant, there should be a step function increase in emission on the cathode side of the grid. To within the uncertainties introduced by the loss of light caused by the grid structure, no such step increase is observed. In this case the cathode current is about 75% of the anode current, as expected from the measured optical transmission of the grid.

V. SUMMARY

The time- and spatial-dependent emission data and the model of the transient experiment presented in this paper support the suggestion of Phelps and Jelenkovic¹ that the excitation of the 811-nm lines of Ar at very high E/n versus is the result of collisions of fast Ar atoms with Ar, where the fast Ar is produced in charge-transfer collisions of fast Ar⁺ with Ar. This result, coupled with the evidence for the dominance of ionization by Ar-Ar collisions in Ar breakdown at very high voltages,¹ provides a reasonably complete picture of the primary processes in Ar discharge at low currents and very high E/n values. However, a number of other problems remain to be solved. First, the excess emission observed¹ in spatial scans near the cathode at moderate E/n values is still unexplained. Second, the discrepancies among the various determinations of electron excitation coefficients used to normalize our relative excitation coefficient data at high E/n values lead to uncertainty in the absolute magnitudes of the derived cross sections for excitation in Ar-Ar collisions.¹

The semiquantitative agreement of the ion and fast-atom model of Sec. III with experiment shows that the concept of the more important fast atoms traveling faster than the ions is useful in explaining the observed emission wave forms. The models used in this paper do not provide detailed electron and fast-atom velocity distributions, time-dependent current, and emission wave forms, etc. Because of the small number of collisions, i.e., < 100 , made by electrons, ions, and fast atoms in crossing the drift tube, the Monte Carlo simulation technique³⁴ would appear to be a good way to improve the models presented in this paper and in Ref. 1.

Finally, we wish to point out that the mechanisms of excitation by fast atoms and excitation of resonance levels by electrons followed by cascading that are the dominant excitation mechanisms in our experiments have not been considered in the analyses of the emission from discharges used in plasma processing, etc.³⁵

ACKNOWLEDGMENTS

The authors wish to acknowledge helpful discussions with A. C. Gallagher, P. J. Chantry, and E. E. Kunhardt. This work was supported in part by the National Institute of Standards and Technology and the Lawrence

Livermore National Laboratories. The participation of D.A.S. was made possible by the Commonwealth Scientific and Industrial Research Organization of Australia.

APPENDIX

This appendix is concerned with the special features of the loss of ions to grids when operated with nonuniform electric field and in gases in which the ions undergo symmetric charge-transfer collisions with the background gas. This subject does not appear to have been discussed in the literature.

Our principal point is that because a symmetric charge-transfer collision can be regarded to a good approximation as resulting in the formation of an ion with thermal energy and random direction, the motion of the

ion after a collision is in the direction of the local electric field. If this field is directed toward the surface of the grid wires, the trajectory of the ion will be toward the grid surface. When the applied electric field is different on the sides of the grid plane the distorted electric field extends over a distance comparable to the grid opening. This means that when the mean free path of the ion is comparable to the grid opening and the electric field is nonuniform in the sense of this paper, we expect significant increase in the loss of ions to the grid compared to that calculated from the optical transparency of the grid. The loss of ions to a grid is expected to be significantly smaller for foreign gas ions than for ions formed from the parent gas because of the generally smaller ion-atom collision cross section and because the persistence of velocity tends to carry the ion in its original direction perpendicular to the grid plane.

*Permanent address: Division of Manufacturing Technology, Commonwealth Scientific and Industrial Research Organization, P. O. Box 218, Lindfield, New South Wales 2070, Australia.

†Also at Department of Physics, University of Colorado, Boulder, Colorado 80309.

¹A. V. Phelps and B. M. Jelenković, *Phys. Rev. A* **38**, 2975 (1988).

²J. P. Molnar, *Phys. Rev.* **83**, 940 (1951); A. V. Phelps and J. P. Molnar, *ibid.* **89**, 1202 (1953).

³R. N. Varney, *Phys. Rev.* **93**, 1156 (1954).

⁴H. Kirsch, *Z. Phys.* **178**, 354 (1964).

⁵H. Raether, *Electron Avalanches and Breakdown in Gases* (Butterworth, Washington, D.C., 1964), Chaps. 4 and 7.

⁶D. A. Scott and A. V. Phelps, *Bull. Am. Phys. Soc.* **32**, 1158 (1987); A. V. Phelps, *Invited Papers from the International Conference on Ionization Phenomena in Gases*, edited by W. T. Williams (Hilger, Bristol, 1987), p. 2.

⁷V. T. Gylys, B. M. Jelenković, and A. V. Phelps, *J. Appl. Phys.* **65**, 3369 (1989).

⁸B. N. Klyarfel'd and L. G. Guseva, *Zh. Tekh. Fiz.* **35**, 306 (1965) [*Sov. Phys.—Tech. Phys.* **10**, 244 (1965)]; B. N. Klyarfel'd, L. G. Guseva, and V. V. Vlasov, *Zh. Tekh. Fiz.* **38**, 1288 (1968) [*Sov. Phys.—Tech. Phys.* **13**, 1056 (1969)]; M. J. Schönhuber, *IEEE Trans. Power Appar. Syst.* **PAS88**, 100 (1969); P. C. Johnson and A. B. Parker, *Proc. R. Soc. London Ser. A* **325**, 529 (1971).

⁹B. M. Jelenković and A. V. Phelps, *Phys. Rev. A* **36**, 5310 (1987).

¹⁰W. L. Wiese, M. W. Smith, and B. M. Glennon, *Atomic Transition Probabilities* (U. S. Department of Commerce, Washington, D.C., 1966), Vol. 1, p. 192.

¹¹A. V. Phelps, B. M. Jelenković, and L. C. Pitchford, *Phys. Rev. A* **36**, 5327 (1987).

¹²A. V. Phelps, *J. Phys. Chem. Ref. Data* (to be published). This paper contains a set of recommended cross sections and spatial excitation and ionization coefficients for Ar⁺ and Ar collisions with Ar. These cross sections and coefficients are very nearly the same as those given in Ref. 1.

¹³W. D. Davis and T. A. Vanderslice, *Phys. Rev.* **131**, 219 (1963); J. E. Lawler, *Phys. Rev. A* **32**, 2977 (1985).

¹⁴J. C. Brenot, D. Dhucq, J. P. Gauyacq, J. Pommier, V. Sidis, M. Barat, and E. Pollack, *Phys. Rev. A* **11**, 1245 (1973).

¹⁵M. Barat, J. Baudon, M. Abignoli, and J. C. Houver, *J. Phys.* **B 3**, 230 (1970); V. Sidis, M. Barat, and D. Dhucq, *ibid.* **8**, 474 (1975).

¹⁶J. D. Williams, J. Geddes, and H. B. Gilbody, *J. Phys. B* **15**, 1377 (1982).

¹⁷P. J. Chantry (private communication).

¹⁸J. Dutton, *J. Phys. Chem. Ref. Data* **4**, 577 (1975).

¹⁹V. E. Golant, *Zh. Tekh. Fiz.* **29**, 756 (1959) [*Sov. Phys.—Tech. Phys.* **4**, 680 (1959)]. We have not found any published experimental electron drift velocity data for such high E/n values.

²⁰For $E/n \approx 18.6$ kTd values of Q_e^i are ≈ 40 times the values of α_p^i/n and α_f^i/n and the effective value (Ref. 1) of $(\gamma_p)_{\text{eff}}$ is 0.05, i.e., the effective ion flux arriving at the cathode is 20 times the electron flux leaving. For these conditions the rate of electron impact ionization would be twice the rate of Ar⁺- and Ar-induced ionization near the cathode and relatively more important nearer the anode. Since we are at voltages and nd values below breakdown, and since the fast-atom flux at the cathode builds up quadratically (Ref. 1) with nd , the ionization by fast neutral atoms in the present experiments is significantly smaller than at breakdown. This discussion is oversimplified since it does not take into account the absorption of particles by the grid and resultant increase in breakdown voltage compared to the experiments in Ref. 1. See Sec. IV B.

²¹A. A. Krutof, *Physica* **7**, 519 (1940); J. Dutton, *J. Chem. Phys. Ref. Data* **4**, 577 (1975); R. R. Abdulla, J. Dutton, and A. W. Williams (unpublished).

²²M. J. Druyvesteyn and F. M. Penning, *Rev. Mod. Phys.* **12**, 87 (1940).

²³A. Gallagher (private communication).

²⁴R. Cooper, F. Grieser, M. C. Sauer, Jr., and D. F. Sangster, *J. Phys. Chem.* **81**, 2215 (1977).

²⁵T. Holstein, *Phys. Rev.* **72**, 1212 (1947); **83**, 1159 (1951).

²⁶A. Chutjian and D. C. Cartwright, *Phys. Rev. A* **23**, 2178 (1981).

²⁷G. P. Li, T. Takayanagi, K. Wakiya, H. Suzuki, T. Ajiro, S. Yagi, S. S. Kano, and H. Takuma, *Phys. Rev. A* **38**, 1240

- (1988).
- ²⁸L. R. Peterson and J. E. Allen, Jr., *Chem. Phys.* **56**, 6068 (1972); E. Eggarter, *ibid.* **62**, 833 (1975); J. Bretagne, G. Calède, M. Legentil, and V. Puech, *J. Phys. D* **19**, 761 (1986).
- ²⁹J. K. Ballou, C. C. Lin, and F. E. Fajen, *Phys. Rev. A* **8**, 1797 (1973). Similar large ratios, but smaller magnitudes have been measured by I. P. Bogdanova and S. V. Yurgenson, *Opt. Spekytosk.* **62**, 471 (1987) [*Opt. Spectrosc. (USSR)* **62**, 281 (1987)].
- ³⁰V. Kempter, G. Riecke, F. Veith, and L. Zehnle, *J. Phys. B* **9**, 3081 (1976).
- ³¹Instrumental time delays of ≈ 60 ns have been measured for this counting chain. V. T. Gyls and A. V. Phelps (unpublished).
- ³²S. Chapman and T. G. Cowling, *The Mathematical Theory of Non-Uniform Gases* (Cambridge University Press, Cambridge, England, 1970), Chap. 13.
- ³³R. S. Robinson, *J. Vac. Sci. Technol.* **16**, 185 (1979).
- ³⁴E. J. Lauer, S. S. Yu, and D. M. Cox, *Phys. Rev. A* **23**, 2250 (1981); A. C. Dexter, T. Farrell, and M. I. Lees, *J. Phys. D* **22**, 413 (1989).
- ³⁵R. A. Gottscho and V. M. Donneley, *J. Appl. Phys.* **56**, 245 (1984); T. Makabe and M. Nakaya, *J. Phys. D* **20**, 1243 (1987); T. Kokubo, F. Tochikubo, and T. Makabe, *ibid.* **22**, 1281 (1989).